A whole-lithosphere view of continental growth

J.R. Reimink, J.H.F.L. Davies, J.-F. Moyen, D.G. Pearson

Supplementary Information

The Supplementary Information includes:

- Methods
- Tables S-1 to S-4
- Figures S-1 to S-11
- Supplementary Information References

Methods

Previous Crustal Growth Estimates

Previous crustal growth estimates calculated by Dhuime *et al.*, (2012; 2017) are here collectively referred to as D27 and these widely used crustal growth curves are based on a modification of the calculations of Belusova *et al*. (2010). In the calculation scheme used by D27, an age spectrum was obtained by compiling zircon Hf-isotope depleted mantle model extraction ages. Each individual zircon U-Pb + Hf isotope data point was used to calculate a depleted mantle model extraction age, and these model ages were binned across geologic time. This age distribution was corrected for reworking using a modification of the methods employed by (Belousova *et al.*, 2010). Instead of considering only zircon Hf isotope data, D27 used zircon O-isotope data to identify crustal reworking signals in the zircon record where zircon oxygen isotope values above the mantle range were considered to be evidence of a reworking signal. A curve proposed to be the crustal growth rate was calculated by determining the relationship between crustal reworking – identified using zircon Hf isotope model ages – and juvenile crustal growth – identified using O-isotope ratios. These calculations are replicated in Supplementary Table S-2. However, there is a flaw in the calculations employed in the D27 work (as pointed out by (Korenaga, 2018)).

The New Crust Generation Rate in the original formulation is calculated by

100 – Crustal Reworking Rate.

The Crustal Reworking Rate was calculated by taking:

100 * (Reworked Crust Ages / (Reworked Crust Ages + Calculated New Crustal Ages))

As this equation shows, the derived value is a ratio of ages, and is therefore non-dimensional (Korenaga, 2018). Thus, the Crustal Reworking Rate value is not in fact a rate, but a ratio of reworked crust / all crust, and likewise the New Crust Generation Rate is not a rate but a ratio of New Crust to Total Crust. These ratios, which by definition must be between 0-1 (or 0-100 when multiplied by 100), cannot be summed over time in a meaningful way; performing a cumulative sum calculation on non-dimensional values between 0-100 is meaningless.

This is best understood when considering a hypothetical example. If 1,000 zircons are formed between 1000-1100 Ma, and 10,000 zircons are formed between 1100-1200 Ma, the goal is to determine how many juvenile zircons formed between 1000 and 1200 Ma. The first step is to determine how many zircons derived from reworked crust and how many formed from juvenile crust. This can be determined by taking the ratio of Reworked Crust / Total Crust, or the number of zircons formed from reworked sources / total number of zircons. Hypothetically assuming that the reworking ratio is 50% in each time interval. To calculate the crustal growth rate, or the cumulative number of juvenile crust ages through time, the cumulative total of the 50% reworking ratio should be multiplied back onto the age distribution to get 500 juvenile zircons between 1000-1100 Ma and 5,000 between 1100-1200 Ma. These zircon ages should be cumulatively summed over this time interval to calculate a juvenile growth rate. Thus, the derived ratios of New Crust/Total Crust must be applied to an age distribution to get cumulative juvenile ages through time, which then can be cumulatively summed to get a growth curve through time. If not, the ratio is just the relative proportion of new crust to reworked crust over time, not the amount of new crust.

Our crustal growth estimate

We take an approach that modifies the D27 calculation by applying a New Crust Generation (Rate) value – the ratio of new crust to total crust at any given time interval – and multiplying this value back onto the age distribution of zircon Hf-isotope depleted mantle model ages. These values, now juvenile zircon ages per time interval, are cumulatively summed through Earth history to yield a model crustal growth rate based on zircon Hf data corrected for crustal reworking using zircon O-isotope data (Fig. S-1). It is important to note that this crustal growth calculation is still underpinned by the Hf-isotope model age distribution, so the method does not solely rely on the major element composition of granitoids or zircon oxygen isotopes through time.

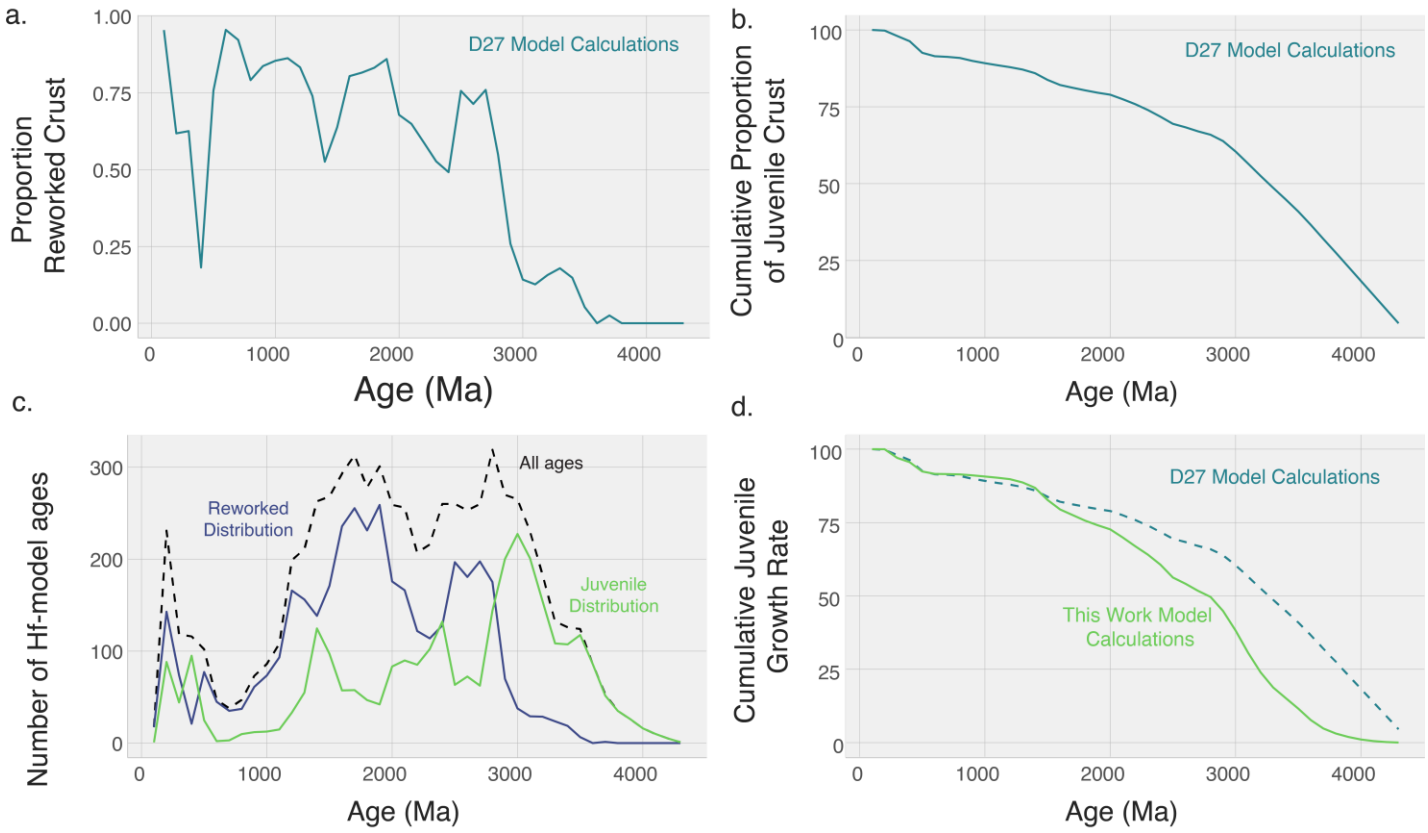

Figure S-1 A figure reproducing the calculations of Dhuime *et al.* (2012) illustrating the error in those calculations. **(a)** Shows the proportion of reworked crust / total crust in each age bin (called Crustal Reworking Rate by Dhuime *et al*., 2012). This is a ratio of reworked to total crust and is therefore limited at 1 – or 100 when multiplied to get a percent. The inverse of this reworking ratio, the ratio of juvenile crust / total crust, was then cumulatively summed to get the curve shown in (b.), **(b)** Shows the cumulative proportion of juvenile crust, not a crustal growth rate. To get an actual growth rate, the proportion of juvenile crust must be multiplied back onto a real age distribution, as done in the bottom panels (c and d). **(c)** Shows the Hf model age distribution from Dhuime *et al*., (2012) in the black dashed curve. The proportion reworked and proportion juvenile (derived from the top left curve) is multiplied onto this age distribution curve to get the number of reworked and juvenile ages in each age bin. This value can then be summed through geological time to get a cumulative juvenile growth rate – the green curve shown in (d). **(d)** Shows the cumulative proportion curve (which is published as a growth rate in D27) as the dashed line to highlight the dramatic difference between the two calculations. Our analysis uses the framework outlined in the lower panels (c and d) using a more recently updated database of Hf model ages (Roberts and Spencer, 2015) and uses whole rock elemental variations instead of less reliable zircon O-isotope ratios to track reworking.

Errors in Quantification of Continental Reworking using Zircon O-isotopes

As discussed in the main text, zircon oxygen isotope ratios are not ideal tracers of crustal reworking. We expand our rationale for this statement here. Two primary reasons cast doubt on the veracity of O isotopes as faithful recorders of reworking 1) the maximum $\delta^{18}O$ value of zircons continue to increase throughout geologic time, and 2) Archean zircon $\delta^{18}O$ values are very limited in range. This combination means that any continental reworking filter based on zircon oxygen isotope ratios does not scale linearly across geologic time

and provides a biased view on crustal reworking. For instance, ongoing crustal reworking in the Archean – detected in the whole rock record (Bucholz and Spencer, 2019; Laurent *et al.*, 2014) and potentially in the ancient zircon record (Ackerson *et al.*, 2021) – is not readily obvious in the zircon O-isotope record.

There may be several reasons for this. First, when considering strongly peraluminous granites (SPGs) derived from nearly pure sediment melting (a classic example of continental reworking) Bucholz and Spencer (2019) show that the source clay mineral content incorporated into SPGs is nearly identical across the Archean-Proterozoic boundary despite a difference in zircon oxygen isotope ratios within the same sample suite. This indicates that oxygen isotopes in these rocks are not tracing a change in the amount of recycled component in the melt. The Bucholz and Spencer (2019) result may be due to variable oxidation states experienced by the sediments prior to melting to form the SPGs as they formed before and after the oxygenation of Earth's atmosphere. Also, Archean sedimentary rocks have been shown to have a more subdued oxygen isotope composition than Phanerozoic sedimentary rocks (Bindeman *et al.*, 2016), potentially related to maturation of the continental crust and the weathering cycle throughout geologic time. Thus, even if the oxygen isotope composition of Archean S-type granites behaved in an identical manner to the modern, the limited range in shale oxygen isotope values would limit the ability of zircon oxygen isotopes to detect reworking.

Another possible issue is that continental reworking is not only generated by sedimentary melting but can also be caused by direct melting of continental igneous rocks. While this process (essentially magmatic differentiation) can shift oxygen isotope ratios in magmatic zircons slightly above the mantle field (Bucholz *et al.*, 2017), it is unlikely to produce zircons with oxygen isotope ratios that are dramatically higher than the mantle composition. Such continental igneous recycling is likely to occur in higher proportions in the Archean Earth, and be potentially undetected by oxygen isotopes in zircon, especially if continental crust was mostly submerged beneath oceans (Bindeman *et al.*, 2018; Dong *et al.*, 2021; Kump and Barley, 2007; Reimink *et al.*, 2021) and did not produce sediments at a similar rate to the modern world.

Thus, zircon oxygen isotope ratios are not accurate trackers of continental reworking throughout Earth history. Zircons formed in magmas derived from continental reworking, in this case in the form of melting sedimentary rocks, are more likely to have subdued oxygen isotope compositions, especially in older samples. This means that a reworking filter based on zircon oxygen isotopes is unreliable and should not be used to assess the relative roles of growth versus re-working through geological time.

Calculating crustal reworking using zircon oxygen isotopes will bias any crustal growth records to artificially rapid early growth rates, particularly in the Archean. For instance, if continental reworking did occur in the Neoarchean (2.5-3.2 Ga), but zircon oxygen isotopes recorded no continental reworking, all ages in the Neoarchean would be classified as juvenile additions to the continental crust.

Tracking Continental Reworking Using the Whole Rock Major Element Compositional Record

The very extensive whole-rock major element compositional record suffers from fewer biases than the zircon oxygen isotope record as a potential tracer of continental reworking. First, there are petrologically imposed limits to the compositional endmembers that occur on Earth. The eutectic granite minimum defines one compositional limit (for most igneous rocks) and the pressure/temperature regimes in the mantle limit the types of magmas produced by partial melting of peridotite. While there is a time-dependency to the latter – for instance komatiite magmas were much more prevalent in the Archean than today (Arndt *et al.*, 2008; Grove and Parman, 2004; Walter, 1998) and sodic granitoids made up a larger fraction of the Archean continental crust than today (Martin, 1986; Moyen and Martin, 2012) – the compositional endmembers have largely

remained fixed. This means that discrete reworking indices will be time-invariant and can be reliably applied across the geologic record. Second, unlike zircons, which are limited in their occurrence to rock-types that have suitable silica activities and alkalinities to crystallise them, the whole rock record is not restricted to a particular end of the rock spectrum. This suggests that using the major element composition of continental rocks may provide a better path to defining reworking through geologic time, assuming that the exposed continental crust is broadly representative of the spectrum of rock compositions at any given time – an assumption implicit in any approach, whether mineralogical or bulk rock, that uses exposed crustal rocks to track continental reworking.

Classic indicators of the melting of sediments, one form of continental reworking, include the aluminum saturation index (ASI), which is similar in function to the classic A/CNK index of (Shand, 1943). The ASI index separates metaluminous from peraluminous melts, and has been used to differentiate granites formed by partial melting of sedimentary rocks, so-called S-type granites, from those derived from melting of igneous protoliths, I-type granites (Chappell and White, 2001; Frost *et al.*, 2001). However, rocks with elevated ASI values can be produced by fractional crystallization of melts formed from melting of igneous protoliths (Frost *et al.*, 2001), while peraluminous melts can contain a mixture of mantle and crustal sources (Collins, 1996; Gray, 1984; Kemp *et al.*, 2007).

To avoid the complexities associated with the ASI classification, Moyen *et al*. (2017) derived a projection that can isolate compositional diversification driven by fractionation versus source variability. The details of this plotting scheme can be found in the supplements to Moyen *et al*. (2017) and (Bonin *et al.*, 2020) but are summarised here briefly. Essentially, the plotting relies on an expansion of the 'closed Shand diagram' to be plotted from biotite compositions and expanded to show more compositional diversity (Figure S-2). This plot results in an open ternary diagram (where compositions can plot outside the ternary boundaries) that has Al+(Na+K) on one apex, Ca+Al on another, and 3Al+2Na+K) on the last. In this space, the A/CNK link runs perpendicular to the Al+(Na+K) apex. To further understand the validity of this plotting projection, Moyen *et al.* (2017) plotted the melt compositions from experimental partial melting reactions, coloured by the starting material composition.

Figure S-2 shows how the Theta parameter is calculated from a whole-rock major element composition. The Theta value (or angle from the horizontal) is very similar to the "alpha" parameter derived in Bonin *et al.* (2020), where a theta value of zero plots along the horizontal A/CNK=1 line. In this plotting space, Moyen *et al.* (2017) showed that experimentally derived melt compositions do not cluster but instead create linear arrays (Figure S-3). Melts derived from sedimentary starting compositions are clearly differentiated from partial melts of mafic rocks. Importantly for our purposes, melts created from felsic crustal sources, an important source of continental reworking that is not captured by the peraluminous/metaluminous definition, can be distinguished from partial melts of mafic (and ultramafic) sources.

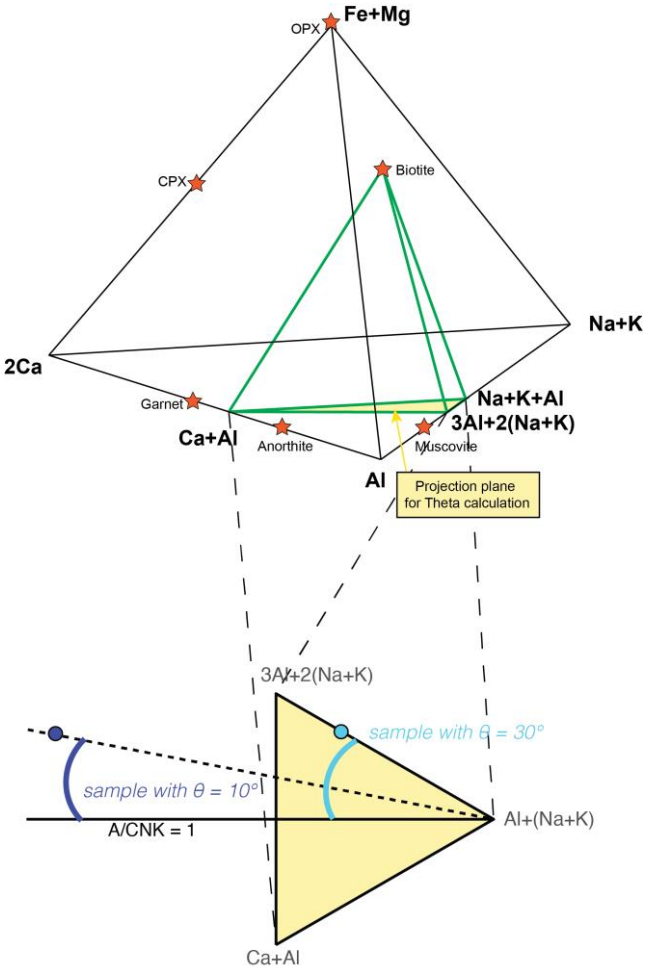

Figure S-2 Representation of the bulk rock major element plotting scheme derived by Moyen *et al*. (2017). The lower yellow triangle shows how the Theta value is calculated, where the blue data point has a theta value of 30 and the purple rock composition has a theta value of 10. A theta of 0 plots along the horizontal A/CNK=1 line. This derivation is very similar to the 'alpha' metric derived in Bonin *et al*. (2020).

Using the distribution of melts produced during partial melting experiments, derived from different starting source compositions, we designed a simple naïve Bayesian classifier to determine the probability that any given rock composition is produced by partial melting of a given source composition. Figure S-3 shows a schematic diagram and example calculation of our Bayesian classifier. Figure S-3a shows the distribution of experimental partial melt compositions, coloured by the starting composition. Figure S-3b shows the kernel density estimate of the theta values for melts generated from each bulk composition. Melts from sedimentary bulk compositions (in yellow) have a peak at 20° theta, while ultramafic compositions (dark purple) have a double peak at ~5° and ~-5°. Fig. S-3b also shows the calculated probability that a rock with Theta=11° (red vertical line, and dashed line in Fig S-3a) was sourced from each bulk compositional category (horizontal coloured lines with probabilities labeled). Figure S-3c shows a table with the raw probabilities for that same rock with Theta=11°, matching the measurements from the y-axis in Figure S-3b. These probabilities are then normalised to the total probability density for that particular rock, and relative probabilities are calculated. Thus, in our calculation, a rock with theta = 11° has an ~8% chance of being derived from a sediment, ~35% chance of being derived from a felsic source, ~12% chance of being sourced from an intermediate rock, ~26% from a mafic source, and ~17% from an ultramafic source. In this way, we apply probabilities to each individual rock composition, which allows us to estimate the source composition while considering the scatter of the experimental melt compositional data.

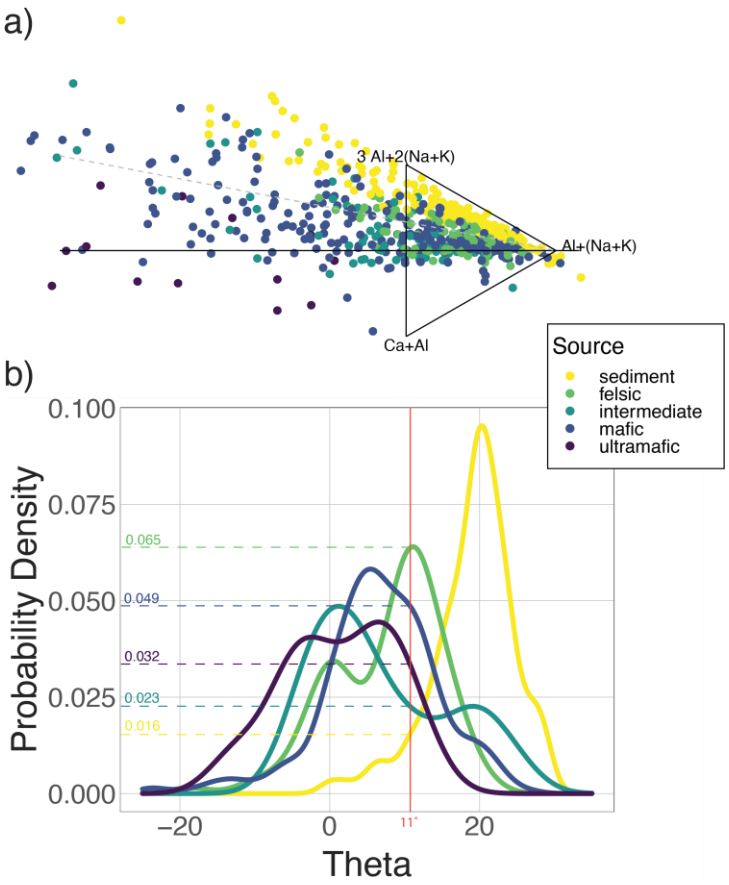

c)

Rock Theta = 11°

Source	Probability Density	Normalized Probability
Sediment	0.016	8.64%
Felsic	0.065	35.1%
Intermediate	0.023	12.4%
Mafic	0.049	26.4%
Ultramafic	0.032	17.3%

Reworked = 56.14%

Figure S-3 Schematic illustration of the naïve Bayesian classifier derived here to estimate the probability any given rock was derived from one of five source categories, based on the compositional plotting derived by Moyen *et al*. (2017) and Bonin *et al*. (2020). See text for a detailed explanation. **(a)** Shows the experimental data compiled in Moyen et al. (2017) colored by source composition. **(b)** Shows the distribution of theta values of the experimental compositions shown in (a), broken apart by source composition, and **(c)** shows the source composition probability estimate breakdown, based on the theta values, for an example rock with a theta value of 11.

Using this naïve Bayesian classifier, we then simplify the five categories down to two – reworked and juvenile. For this analysis, we are simply attempting to determine the probability a given rock represents reworked continental crust. To do this, we sum up the probability in the sedimentary, felsic, and intermediate source categories. The remaining percentage is the probability a given rock is from a juvenile source. Figure S-4

shows the breakdown of probability density and normalised probability for rock compositions across a range of theta values.

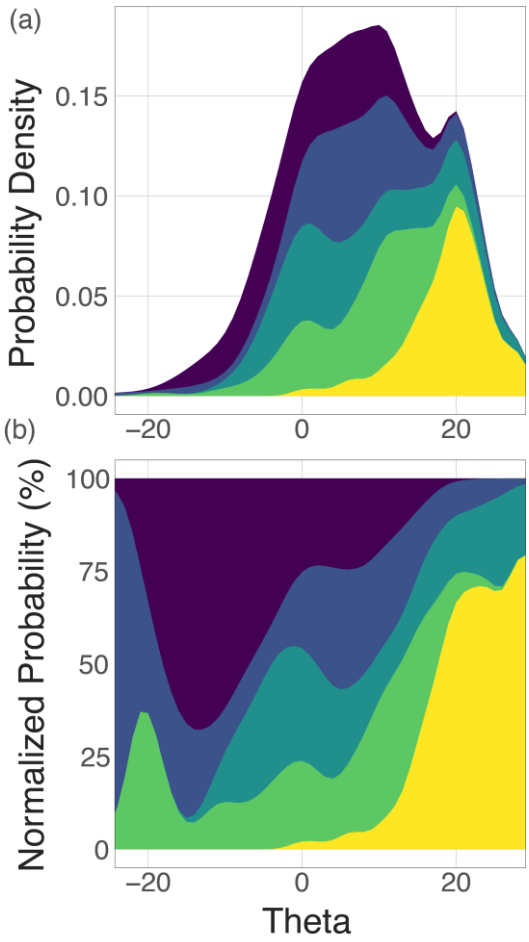

Figure S-4 Probabilities output from our naïve Bayesian classifier for a range of rock theta values. **(a)** Shows the raw probability density across the theta values, and **(b)** shows the normalised probability, in percent, for each theta value.

Moyen *et al.* (2017) showed that rocks from the French Massif Central (FMC) generally have highly positive theta values (following the terminology we use here). Figure S-5 shows the results of our calculations for both the FMC samples and those from the Kohistan Arc Batholith (Jagoutz, 2014). Our probability-based calculation assigns high probability to the FMC suite sample being reworked, with the Kohistan Arc Batholith being significantly less likely to be derived from reworking of pre-existing felsic crust. While our model suggests that there is some probability that individual Kohistan rocks may represent reworking, there exists a substantial difference between the probability of reworking for these rocks compared to FMC suite rocks (Fig. S-5). Additionally, as discussed below, systematic offsets in reworking will not substantially modify our crustal growth rate calculations – only age-varying errors will change this.

Therefore, to calculate reworking probabilities, igneous whole rock data must be compared to the experimental database shown by Moyen *et al*. (2017). We have done this for each sample in the (Gard *et al.*, 2019) igneous rock compilation, and then determined the probability of reworking for each sample.

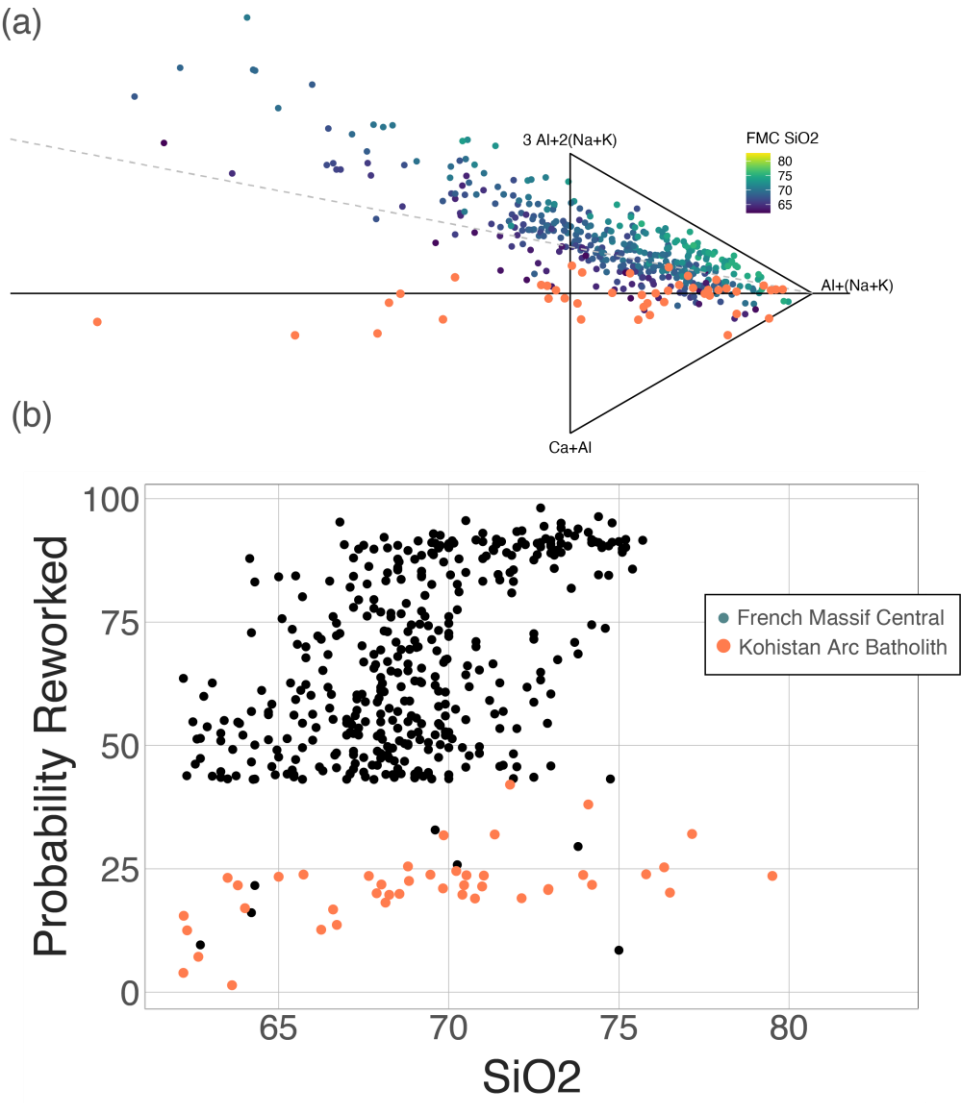

Figure S-5 Whole-rock data from the French Massif Central from Moyen *et al.* (2017, as well as Kohistan Batholith samples plotted in the theta compositional framework in **(a)** and shown with each samples calculated probability of being reworked crust in **(b).** Igneous rocks from the French Massif Central were formed by reworking of continental crust, while the Kohistan Arc Batholith was formed in a juvenile arc environment derived from juvenile mantle melts (Jagoutz, 2014). The data shown in this plot are from Moyen *et al.* (2017) and references are found in that work; the FMC data points in (a) are coloured according to their SiO_2 content while those in (b) are black, due to SiO_2 being shown in the x-axis.

We then calculate the proportion of re-worked crust in 100 Ma age bins (Figs. 1-2) by calculating the ratio of reworked/juvenile rock types within each age interval. The proportion of juvenile rocks through time is shown in Fig. 2 as a moving average, calculated in 250 Ma moving windows in 25 Ma increments. The database used for these calculations is accessible as Supplementary Table S-1. We also plot the difference between our theta metric and the ASI values calculated for each rock (Fig. S-6), which shows that in general samples with theta values between 10 and 30 (here considered to represented re-worked sources) have high ASI, but not universally. The correlation is not perfect, because these theta values may be produced by melting of igneous sources rather than sediments, which is also a crustal re-working process.

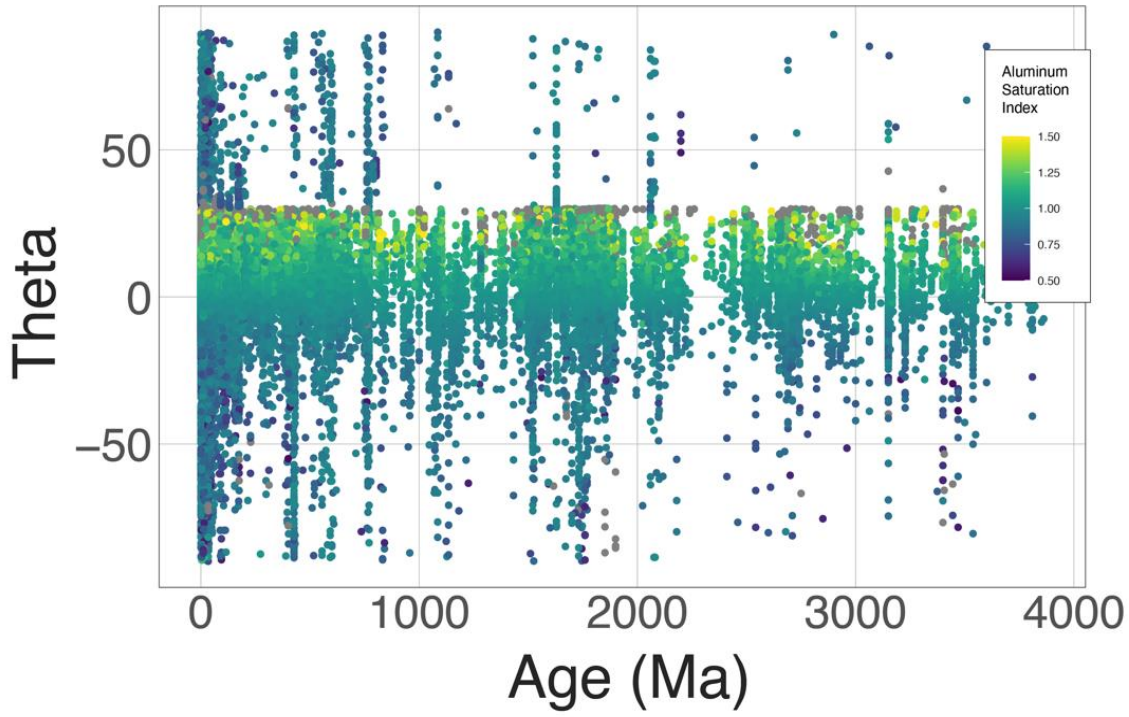

Figure S-6 The whole rock igneous database (Gard *et al*., 2019), filtered for SiO_2 > 62 wt.%, and filtered for samples with complete major element data. The symbols are coloured for their ASI value, and the correlation between Thetas of 10-30 and relatively high ASI values can be seen. Note that not all rocks with theta between 10-30 degrees have high ASI values as melting of felsic igneous material also yields a theta value in this range, without producing a rock with high ASI, though these melting products still represent reworking of continental material. Theta values >30 wrap around the plotting space and there is a smooth transition from Theta = 90 to Theta = -90.

To calculate the reworking fraction through time shown in Figure 2 of the manuscript, we performed the following calculation. First, the normalised probabilities for each of the five source categories was calculated for each rock composition. Then these rock samples were divided into 100 Ma age bins (or used in the moving average calculation – Fig. 2) and the total probability for each of the five categories was summed across each age bin. These summed probabilities were grouped into 'reworked' and 'juvenile' categories by adding the probabilities of a given rock being derived from a 'sediment', 'felsic', or 'intermediate' source categories together (reworked) and adding 'mafic' and 'ultramafic' categories together to get 'juvenile'. These final summed probabilities were then normalised to calculate the reworking fraction of that age bin.

Sensitivity Testing in Relation to Calculated Crustal Growth Curves

Importantly, our calculation is not dependent on the number of preserved rock samples through time, only on the distribution of rocks derived from juvenile sources and those derived from continental reworking. This is shown in Figure 3 by a calculation of continental growth rates using a whole-rock database that includes a modelled Mesoarchean-Hadean continental crust.

To perform our modelled Mesoarchean-Hadean crust calculation, we modelled >3.2 Ga continental rocks as equivalent in number and distribution to those preserved from the Neoarchean – of which there is a globally-

representative set of samples in the (Gard *et al.*, 2019) database. Figure S-7 shows the number of samples over time used for this paper.

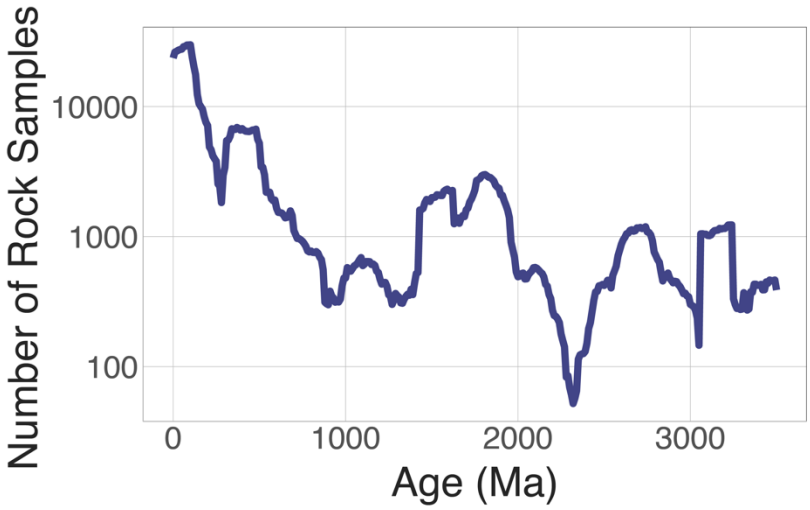

Figure S-7 The number of samples in the whole-rock database, calculated in a moving window that replicates the calculation for the reworking index shown in Fig. 3 of the manuscript.

Figure 3 of the main text shows the continental growth curve calculated by correcting for continental reworking using a synthetic Archean-Hadean rock record, and Supplementary Table S-2 to S-4 show the calculations that yield curves plotted in Figure 3. However, in order to fully test the sensitivity of our approach, we show two more calculations. Both of these calculations aim to test the influence of crustal reworking on the continental growth rates calculated here. First, we aimed to determine how much influence the calculated reworking rates had on our derived crustal growth rates. For instance, our Theta whole-rock reworking calculation clearly has the potential to be biased towards more reworking, as evidenced by our naïve Bayesian classifier applied to the Kohistan arc batholith (Fig. S-5) which showed low probabilities of 'reworked crust' in this location – well known to be comprised of juvenile crustal packages (Jagoutz, 2014).

To test the influence of potential systematic biases in our reworking calculation, we performed the same suite of crustal growth rate calculations using, instead of our calculated reworking rate (Fig. 2), extreme choices for uniform crustal reworking rates of 99% and 1% (0.99 and 0.01) across the entire span of geologic time. These extreme reworking rates were multiplied back onto the Hf-isotope database as in Figure S-1. Figure S-8 shows the results of these calculations and their influence on the resulting crustal growth curves. The left panel shows the reworking fractions used in our calculation, and the right panel shows the calculated growth rates using the three reworking fractions, 0.01 (constant through time), 0.99 (constant through time), and the Theta value. As shown in the right panel, our calculation is relatively insensitive to the raw reworking value used through time. In other words, even if our Theta value reworking metric was systematically biased – for instance overestimating reworking as in the Kohistan example – it would not substantially affect our calculated growth rates.

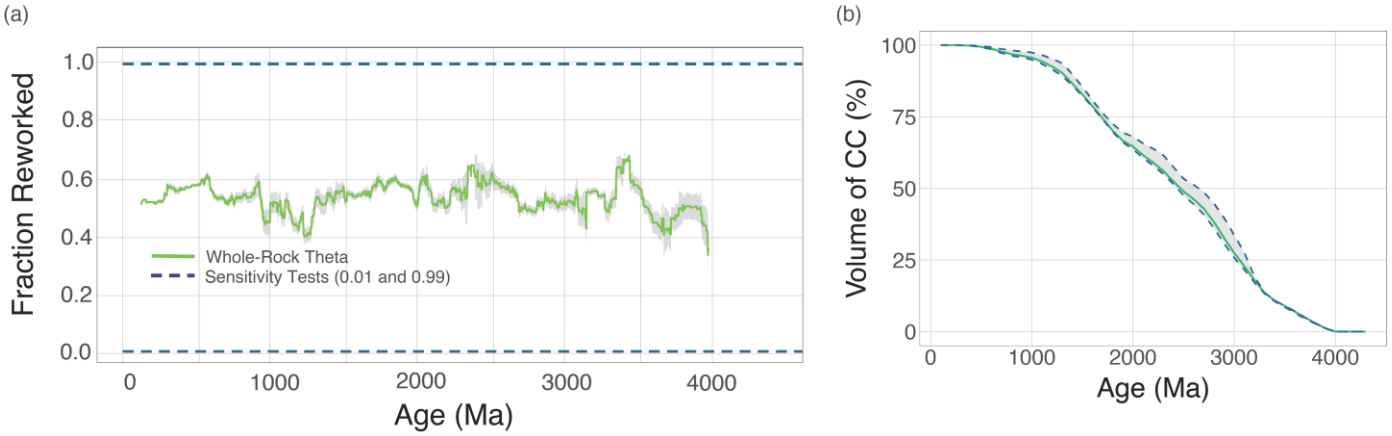

Figure S-8 A sensitivity test showing the effect of systematic bias in reworking propagated onto our crustal growth curves. **(a)** shows the crustal reworking fraction as determined by the whole rock record, and synthetic reworking estimates of 0.01 and 0.99. **(b)** shows the results of these reworking estimates propagated through the crustal growth curve. Even in the instance of an extreme bias (0.99 reworking through time) there is no significant change in the crustal growth rate calculated here (right panel where the y-axis shows the fraction of continental crust normalised to present). Therefore our calculation is relatively insensitive to systematic biases in crustal reworking.

Secondly, we test the sensitivity of our crustal growth rate calculation to temporal biases in the theta calculation. To do this, we again perform the same calculation with an extreme set of hypothetical reworking estimates. Figure S-9 shows the results of this test. First, we calculated crustal growth rates by assuming that the Archean (>2.5 Ga) had a low reworking rate of 0.10 and the post-Archean had a higher reworking rate of 0.80. This calculation is shown by the purple curve in Fig. S-9. Next we calculated the crustal growth rate for a hypothetical reworking rate where the Archean had a higher reworking rate (0.80) and the post-Archean was lower (0.10). There is significant offset between these two curves (Fig. S-9). However, our Theta reworking index shows no signs for a systematic bias across the Archean, or any other, geologic boundary in Earth history. This is contrary to the zircon $\delta^{18}O$ reworking tracer which, as discussed above, is a temporally biased reworking indicator and should not be used as a reliable tracer throughout Earth history.

The above tests show that our Theta reworking indicator and the resulting crustal growth curves are not dramatically affected by any systematic bias in the reworking metric (Fig. S-8), and they are only sensitive to time-varying biases which are unlikely to be present in our whole-rock based metric (Fig. S-9), contrary to the commonly used zircon based reworking filter.

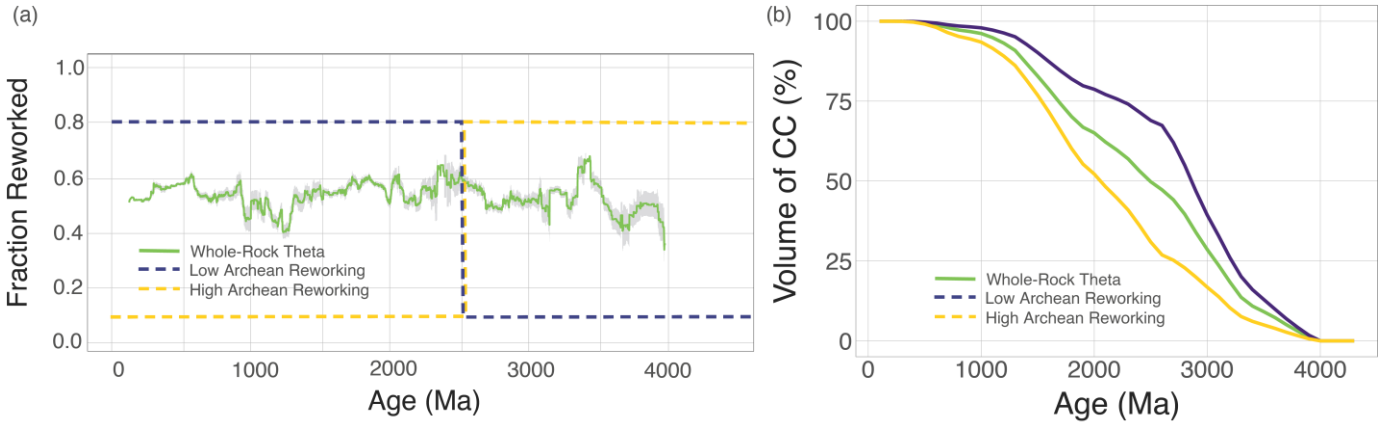

Figure S-9 A sensitivity test showing the effect of time-varying bias in reworking propagated onto our crustal growth curves. **(a)** Shows the reworking fractions through time. The purple curves show the effect of a low (0.10) Archean reworking fraction followed by a step function change to high (0.80) reworking fraction post-Archean. As shown in **(b),** this produces a more rapid crustal growth rate followed by an inflection point in the Archean-Proterozoic boundary. Conversely, the yellow lines show the effect of high (0.80) Archean reworking followed by low post-Archean reworking (0.10). Our whole-rock Theta approach to quantifying crustal reworking shows no evidence for a time-varying bias in the reworking rate.

Uncertainty in the Mantle Age Distribution

The cratonic mantle age distribution shown in Fig. 1 is from a recently published database of cratonic lithosphere ages (Pearson *et al.*, 2021). The data plotted in Fig. 1 are the distribution of samples that were categorised as unmodified cratonic lithosphere ages. We generated uncertainties in the cumulative mantle age curve by resampling the underlying Re-depletion age (TRD) database incorporating uncertainties of +/-200 Ma for each TRD calculation. For the 913 TRD ages in the Pearson *et al.* (2021) database, we recalculated the age for each TRD by randomly selecting an age within a Gaussian uncertainty distribution. For example, for a sample with a TRD age of 2000 Ma, we would select an age randomly from a distribution with a mean of 2000 Ma and a standard deviation of 100 Ma. This was done for each sample with a TRD age in the database and a cumulative distribution was calculated. This process was repeated 100 times to estimate the range of cumulative age distributions that are possible within uncertainty (Figure S-10).

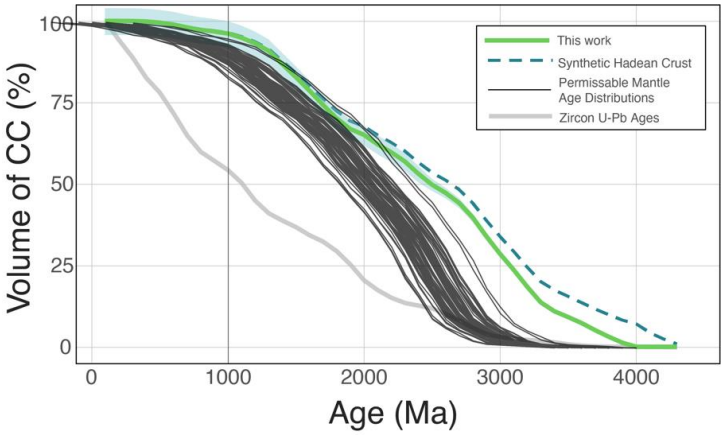

Figure S-10 Resampling of the mantle age distributions conducted to incorporate analytical and calculation uncertainty.

Implications of Alteration on Whole-Rock Reworking Signals

Whole-rock compositions, particularly those from the ancient rock record, are susceptible to chemical overprinting by metamorphism and/or weathering. While our analysis, like all compilations, relies on the original publications to obtain reliable geochemical data from relatively-well preserved rock samples, we must evaluate the impact of chemical overprinting on our whole-rock reworking estimate. Figure S-11 shows one example of this. In this analysis we calculate the reworking index for a suite of chemically altered granites from the original definition of the Chemical Alteration Index (Nesbitt and Young, 1982). The alteration signature moves data points well outside of the plotting area and as such are easily identified as altered. Any whole rock analyses in the data base that plotted well outside of the triangular field were removed as possible alteration. It is important to note that the plotting space shown in these plots are projected from other compositional space, so the actual theta value derived is dependent on other elements/oxides such as FeO in the whole rock. This is by design and calibrated to the mineralogy of the sample (Bonin *et al.*, 2020).

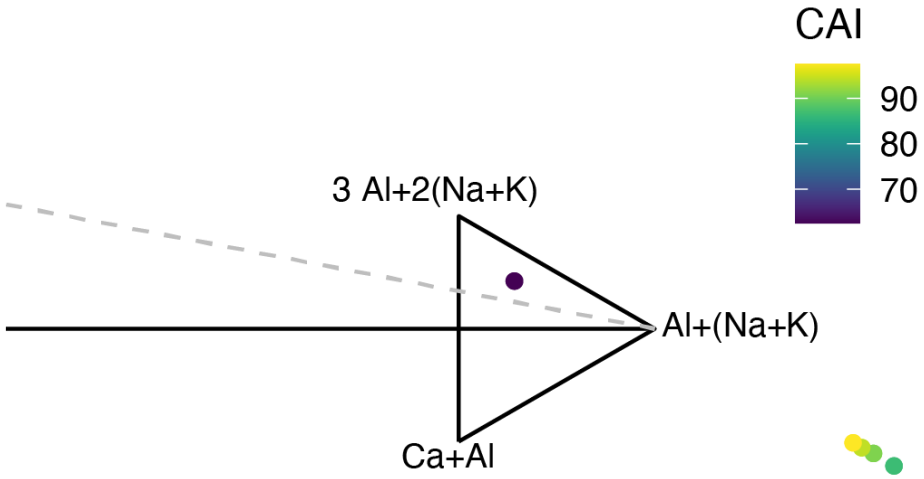

Figure S-11 Altered granite samples projected in the whole-rock reworking plotting space. The dark data point is the unaltered granite sample, while the altered samples are shown in the lower right outside of the plotting area, where CAI is the Chemical Alteration Index and is a metric used to track chemical weathering.

Supplementary Tables

The supplementary tables outline the various models of crustal growth rate, with calculations embedded. Each sheet in the downloadable Excel file represents a different crustal growth rate calculation using various reworking metrics.

Table S-1 Crustal reworking fraction through time calculated in this work and plotted in figures throughout this manuscript.
Table S-2 Dhuime *et al.* (2012) crustal growth rate calculations reproduced for clarity.
Table S-3 Whole-rock based crustal growth rates calculated in this work.
Table S-4 Crustal growth rate models using a synthetic Hadean crust model to test the sensitivity of our calculations.

Tables S-1 through **S-4** (.xlsx) are available for download from the online version of this article at https://doi.org/10.7185/geochemlet.2324.

Supplementary Information References

Ackerson, M., Trail, D., Buettner, J. (2021) Emergence of peraluminous crustal magmas and implications for the early Earth. *Geochemical Perspectives Letters* 17, 50-54. https://doi.org/10.7185/geochemlet.2114

Arndt, N., Lesher, M.C., Barnes, S.J. (2008) *Komatiite*. Cambridge University Press. 487p https://doi.org/10.1017/CBO9780511535550

Belousova, E.A., Kostitsyn, Y.A., Griffin, W.L., Begg, G.C., O'Reilly, S.Y., Pearson, N.J. (2010) The growth of the continental crust: Constraints from zircon Hf-isotope data. *Lithos* 119, 457-466. https://doi.org/10.1016/j.lithos.2010.07.024

Bindeman, I.N., Bekker, A., Zakharov, D.O. (2016) Oxygen isotope perspective on crustal evolution on early Earth: A record of Precambrian shales with emphasis on Paleoproterozoic glaciations and Great Oxygenation Event. *Earth and Planetary Science letters* 437, 101-113. https://doi.org/10.1016/j.epsl.2015.12.029

Bindeman, I.N., Zakharov, D.O., Palandri, J., Greber, N.D., Dauphas, N., Retallack, G.J., Hofmann, A., Lackey, J.S., Bekker, A. (2018) Rapid emergence of subaerial landmasses and onset of a modern hydrologic cycle 2.5 billion years ago. *Nature* 557, 545–548. https://doi.org/10.1038/s41586-018-0131-1

Bonin, B., Janoušek, V., Moyen, J.-F. (2020) Chemical variation, modal composition and classification of granitoids. *Geological Society, London, Special Publications* 491, 9–51. https://doi.org/10.1144/SP491-2019-138

Bucholz, C.E., Jagoutz, O., Jagoutz, O.E., VanTongeren, J.A., Setera, J., Wang, Z. (2017) Oxygen isotope trajectories of crystallizing melts: Insights from modeling and the plutonic record. *Geochimica et Cosmochimica Acta* 207, 154-184. https://doi.org/10.1016/j.gca.2017.03.027

Bucholz, C.E., Spencer, C.J. (2019) Strongly Peraluminous Granites across the Archean–Proterozoic Transition. *Journal of Petrology* 60, 1299–1348. https://doi.org/10.1093/petrology/egz033

Chappell, B.W., White, A.J.R. (2001) Two contrasting granite types: 25 years later. *Australian Journal of Earth Sciences* 48, 489–499. https://doi.org/10.1046/j.1440-0952.2001.00882.x

Collins, W.J. (1996) Lachlan Fold Belt granitoids: products of three-component mixing. *Earth and Environmental Science Transactions of the Royal Society of Edinburgh* 87, 171–181. https://doi.org/10.1017/S0263593300006581

Dhuime, B., Hawkesworth, C.J., Cawood, P.A., Storey, C.D. (2012) A Change in the Geodynamics of Continental Growth 3 Billion Years Ago. *Science* 335, 1334-1336. https://doi.org/10.1126/science.1216066

Dhuime, B., Hawkesworth, C.J., Delavault, H., Cawood, P.A. (2017) Continental growth seen through the sedimentary record. *Sedimentary Geology* 357, 16-32. https://doi.org/10.1016/j.sedgeo.2017.06.001

Dong, J., Fischer, R.A., Stixrude, L.P., Lithgow-Bertelloni, C.R. (2021) Constraining the Volume of Earth's Early Oceans With a Temperature-Dependent Mantle Water Storage Capacity Model. *AGU Advances* 2, e2020AV000323. https://doi.org/10.1029/2020AV000323

Frost, B.R., Barnes, C.G., Collins, W.J., Arculus, R.J., Ellis, D.J., Frost, C.D. (2001) A Geochemical Classification for Granitic Rocks. *Journal of Petrology* 42, 2033-2048. https://doi.org/10.1093/petrology/42.11.2033

Gard, M., Hasterok, D., Halpin, J.A. (2019) Global whole-rock geochemical database compilation. *Earth System Science Data* 11, 1553–1566. https://doi.org/10.5194/essd-11-1553-2019

Gray, C.M. (1984) An isotopic mixing model for the origin of granitic rocks in southeastern Australia. *Earth and Planetary Science Letters* 70, 47–60. https://doi.org/10.1016/0012-821X(84)90208-5

Grove, T.L., Parman, S.W. (2004) Thermal evolution of the Earth as recorded by komatiites. *Earth and Planetary Science Letters* 219, 173-187. https://doi.org/10.1016/S0012-821X(04)00002-0

Jagoutz, O. (2014) Arc crustal differentiation mechanisms. *Earth and Planetary Science Letters* 396, 267-277. https://doi.org/10.1016/j.epsl.2014.03.060

Kemp, A.I.S., Hawkesworth, C.J., Foster, G.L., Paterson, B.A., Woodhead, J.D., Hergt, J.M., Gray, C.M., Whitehouse, M.J. (2007) Magmatic and crustal differentiation history of granitic rocks from Hf-O isotopes in zircon. *Science* 315, 980-983. https://doi.org/10.1126/science.1136154

Korenaga, J. (2018) Estimating the formation age distribution of continental crust by unmixing zircon ages. *Earth and Planetary Science Letters* 482, 388-395. https://doi.org/10.1016/j.epsl.2017.11.039

Kump, L.R., Barley, M.E. (2007) Increased subaerial volcanism and the rise of atmospheric oxygen 2.5 billion years ago. *Nature* 448, 1033-1036. https://doi.org/10.1038/nature06058

Laurent, O., Martin, H., Martin, H., Moyen, J.F., Moyen, J.-F., Doucelance, R., Doucelance, R. (2014) The diversity and evolution of late-Archean granitoids: Evidence for the onset of "modern-style" plate tectonics between 3.0 and 2.5Ga. *Lithos* 205, 1-82. https://doi.org/10.1016/j.lithos.2014.06.012

Martin, H. (1986) Effect of steeper Archean geothermal gradient on geochemistry of subduction-zone magmas. *Geology* 14, 753–756. https://doi.org/10.1130/0091-7613(1986)14<753:EOSAGG>2.0.CO;2

Moyen, J.-F., Martin, H. (2012) Forty years of TTG research. *Lithos* 148, 312-336. https://doi.org/10.1016/j.lithos.2012.06.010

Nesbitt, H.W., Young, G.M. (1982) Early Proterozoic climates and plate motions inferred from major element chemistry of lutites. *Nature*. https://doi.org/10.1038/299715a0

Pearson, D.G., Scott, J.M., Liu, J., Schaeffer, A., Wang, L.H., van Hunen, J., Szilas, K., Chacko, T., Kelemen, P.B. (2021) Deep continental roots and cratons. *Nature* 596, 199–210. https://doi.org/10.1038/s41586-021-03600-5

Reimink, J.R., Davies, J.H.F.L., Ielpi, A. (2021) Global zircon analysis records a gradual rise of continental crust throughout the Neoarchean. *Earth and Planetary Science Letters* 554, 116654. https://doi.org/10.1016/j.epsl.2020.116654

Roberts, N.M.W., Spencer, C.J. (2015) The zircon archive of continent formation through time. *Geological Society, London, Special Publications* 389, 197–225. https://doi.org/10.1144/SP389.14

Shand, S.J. (1943) *Eruptive rocks: Their genesis, composition, and classification, with a chapter on meteorites*. J. Wiley & sons, Incorporated.

Walter, M.J. (1998) Melting of Garnet Peridotite and the Origin of Komatiite and Depleted Lithosphere. *Journal of Petrology* 39, 29-60. https://doi.org/10.1093/petroj/39.1.29